JAMES | Journal of Advances in Modeling Earth Systems

RESEARCH ARTICLE
10.1029/2022MS003088

Key Points:

- Two types of planetary boundary layer (PBL) schemes are evaluated in hurricane conditions using a recently developed modeling framework
- *K*-profile parameterization PBL schemes are inherently flawed in hurricane boundary layers
- The Mellor–Yamada–Nakanishi–Niino scheme performs well in hurricane conditions due to its high-order closure and sophisticated parameterization of mixing length

Correspondence to:
X. Chen,
xiaomin.chen@noaa.gov

Citation:
Chen, X. (2022). How do planetary boundary layer schemes perform in hurricane conditions: A comparison with large-eddy simulations. *Journal of Advances in Modeling Earth Systems*, *14*, e2022MS003088. https://doi.org/10.1029/2022MS003088

Received 15 MAR 2022
Accepted 30 SEP 2022

How Do Planetary Boundary Layer Schemes Perform in Hurricane Conditions: A Comparison With Large-Eddy Simulations

Xiaomin Chen[1,2]

[1]NOAA/OAR/Atlantic Oceanographic and Meteorological Laboratory, Miami, FL, USA, [2]Northern Gulf Institute, Mississippi State University, Stennis Space Center, Starkville, MS, USA

Abstract Parameterizations of turbulent processes in planetary boundary layer (PBL) schemes impact tropical cyclone (TC) forecasts. Existing PBL schemes are mostly designed for low-wind conditions, and assessing their uncertainties in hurricane conditions remains challenging, mostly due to very scarce observations. Using a recently developed framework based on large-eddy simulations (LES), this study evaluates *K*-profile parameterization (KPP) and high-order PBL schemes in hurricane conditions. Among KPP PBL schemes, the Global Forecast System (GFS) scheme tends to produce excessively deep inflow layers with large values of eddy viscosity (K_m). Opposite results are found for the Yonsei University (YSU) scheme. Using LES results as a benchmark, the performance of YSU and GFS schemes is improved by modifying the "shape parameter" such that K_m is maximized closer to the surface, and by using a new definition of boundary layer height tailored to high-wind conditions. The LES results also suggest an asymptotic mixing length of ~40 m can improve the Louis-type parameterizations of the YSU scheme that operates above the boundary layer. Among high-order PBL schemes, the Mellor–Yamada–Nakanishi–Niino (MYNN) scheme produces reasonably accurate vertical profiles of eddy viscosity, turbulent stress, and boundary layer winds under different high-wind conditions. Further analysis of MYNN supports a "three-layer" strategy for the mixing length parameterization for TCs that represents different types of turbulent regimes. In contrast, the high-order eddy-diffusivity mass-flux scheme produces excessive boundary-layer vertical mixing and a deeper inflow layer, partly attributable to a notable overestimation of the maximum allowable mixing length in the PBL code.

Plain Language Summary Turbulence is made up of random and continuously changing wind. The energy and momentum exchange between the ocean and the lowest ~1 km atmosphere (i.e., planetary boundary layer or PBL) is through turbulent processes. The size of turbulent eddies, however, is much smaller than the grid spacings of mesoscale numerical models, and thus cannot be directly resolved by model grids. Therefore, parameterizations of boundary-layer turbulence (or PBL schemes) are involved to mimic the turbulent processes on these small scales. These PBL schemes are typically designed for low-wind conditions, and uncertainties of directly applying them to high-wind conditions like hurricanes are not well known, in part due to very scarce turbulence measurements in hurricane boundary layers. This study uses a recently developed modeling framework based on large-eddy simulation (where model grids are small enough to resolve turbulence) to evaluate two types of PBL schemes in hurricane conditions. The framework reveals the pros and cons of each PBL scheme. Using this insight, we recommend suitable PBL schemes for tropical cyclone (TC) modeling and propose solutions to address identified issues in these PBL schemes. These findings provide valuable guidance to the development of PBL schemes in high-wind conditions that may improve TC forecasts.

1. Introduction

Tropical cyclones (TCs) have caused over $1.1 trillion total damage and 6,697 deaths in the US between 1980 and 2021, making them the costliest and deadliest weather disaster in the nation (https://coast.noaa.gov/states/fast-facts/hurricane-costs.html). However, accurately predicting the intensity change of TCs remains challenging. One major reason for this is the poor understanding and modeling of planetary boundary layer (PBL) processes (e.g., Braun & Tao, 2000; Emanuel, 2017; Hill & Lackmann, 2009; Kepert, 2012; Nolan et al., 2009; Smith & Thomsen, 2010). The existing PBL schemes are generally designed for convective boundary layers or low-wind conditions, while turbulence characteristics in those conditions are distinct from those in high-wind, TC boundary layers (Bryan et al., 2017; Chen & Bryan, 2021). In convective boundary layers, turbulence is predominantly

buoyancy-driven, and the vertical velocity variance is maximized in the middle boundary layer (Moeng & Sullivan, 1994). These findings lay the foundation for the development of many PBL schemes [for example, *K*-profile parameterization (KPP) schemes] that have been widely used in research and forecast models. In TC boundary layers, however, turbulence is predominantly shear-driven, and buoyancy plays a role mainly in the upper boundary layer where vertical wind shear weakens (Bryan et al., 2017). Thus, the suitability of using these schemes, which were designed for low-wind conditions, in TC simulations requires a careful examination.

Previous simulation studies assessed the effect of different PBL schemes on the TC intensity and structure using a three-dimensional full physics model (e.g., Braun & Tao, 2000; Chen, Xue, et al., 2021; Smith & Thomsen, 2010). Evaluation based on the full physics model, however, has limitations to attribute the differences in the simulated TCs solely to the different parameterizations in the PBL schemes, in part due to the complex interactions with radiation, microphysics, and other physical processes.

In comparison, Kepert (2012) evaluated various types of PBL schemes in the framework of a steady-state and height-resolving boundary layer model where the pressure at the top of the boundary layer is prescribed. His study recommended the Louis-type scheme, which is a first-order closure and diffusivity at a given point depends only on local conditions, and high-order PBL scheme, which includes prognostic equations for turbulence quantities such that diffusivity at a given point depends not only on local conditions but also on advective and transport processes, for TC simulations. The KPP schemes were found to produce the largest vertical eddy viscosity with a predefined boundary layer depth of 1,500 m, which is in line with the report of excessive turbulent mixing in the Medium-Range Forecast (Braun & Tao, 2000; Noh et al., 2003; Smith & Thomsen, 2010) and Global Forecast System (GFS) (Gopalakrishnan et al., 2013; Zhang et al., 2015) PBL schemes. In this framework, the diagnosed mixed layer depth—that is, the PBL height definition from the Yonsei University (YSU) scheme (see Table 1)—is ∼2 km, which is much larger than the values typically observed in mature hurricanes using the same PBL height definition (≈500–1,000 m, Zhang, Rogers, et al., 2011). This comparison suggests the thermodynamic conditions in Kepert's study differ notably from those in real hurricane boundary layers. Additionally, the fixed boundary layer height in Kepert's framework is a shortcoming for the evaluation of PBL schemes that depend crucially on the diagnosed boundary layer height, such as the YSU and GFS schemes.

In recognition of these issues, this study uses a recently developed evaluation framework tailored to the TC boundary layer (Chen, Bryan, et al., 2021) to assess the performance of various PBL schemes and uncertainties in the parameterizations of boundary layer properties. Building upon a simple method of simulating wind profiles in the boundary layer of TCs (Bryan et al., 2017), this framework uses composite in situ dropsonde data collected in mature hurricanes as the initial conditions to drive large-eddy simulations (LES), which do not require PBL parameterizations, and single-column model (SCM) simulations using different PBL schemes. The LES under realistic thermodynamic conditions provides robust information on turbulence variables in hurricane conditions, which was demonstrated in Chen, Bryan, et al. (2021). It should be noted that eddy viscosity estimation based on in situ flux measurements in the TC boundary layer is rare due to safety and practical considerations. So far, the observed vertical profiles of eddy viscosity are only available in the outer region of TC circulations where the surface wind is relatively weak (18–30 m s^{-1}, Zhang & Drennan, 2012). The insights gained from the LES output can help reveal the intrinsic pros and cons of the PBL schemes. We further propose potential solutions to improve the KPP PBL schemes in hurricane conditions. These results should benefit the TC operational and research communities.

2. Data and Methods

2.1. An Evaluation Framework for PBL Schemes, Model Setup, and Observational Data

In this study, we use the modeling framework developed by Chen, Bryan, et al. (2021) to evaluate two types of PBL schemes in hurricane conditions. This framework allows for a small-domain (∼5 km) LES and a SCM simulation using a PBL scheme under the same controlled thermodynamic and kinematic conditions without the complexities involved in real-data cases and/or evolving TCs. The domain-averaged profiles of turbulence properties and winds from LES are then treated as the benchmark for the evaluation of PBL schemes. LES is treated as the benchmark also because observed profiles of turbulence properties (such as eddy viscosity) are unavailable at hurricane-force wind speeds as discussed earlier. Of note, this framework applies to the region

outside the eyewall since it builds upon a simple method (Bryan et al., 2017) that includes special assumptions related to vertical motions.

Cloud Model 1 (CM1; Bryan & Fritsch, 2002) is used in this study for both the LESs and SCM simulations. For LES, there are 528 × 528 grid points horizontally, and the horizontal grid spacing is 10 m. We use 500 vertical levels, with the model top of 3 km. The vertical grid spacing is 5 m below 2 km and increases gradually to 12.5 m between 2 and 3 km. For SCM simulations, a very similar model setup is used except that the vertical grid spacing is 20 m below 2 km and increases gradually to 50 m between 2 and 3 km. Three sets of simulations are performed, using thermodynamic profiles outside the eyewall of mature hurricanes where the 10-m tangential wind is approximately 25 m s^{-1} (V25 hereafter), 35 m s^{-1} (V35 hereafter), and 45 m s^{-1} (V45 hereafter), respectively. These profiles are derived from a composite analysis of dropsonde data collected during research and operational flights conducted by NOAA P3 and G-IV, NASA DC-8 and G-IV, and Air Force C130 aircraft in category 4–5 hurricanes between 1990 and 2010. The LES domain or SCM grid point is located due east of the storm center, and u and v hereafter denote radial and tangential winds, respectively. For SCM simulations, the horizontal grid spacing is set to 4 km, which is beyond the model gray zone where the scale-aware effect is activated in specific PBL schemes, including Mellor–Yamada–Nakanishi–Niino (MYNN) and turbulence kinetic energy (TKE)-based eddy-diffusivity mass-flux (EDMF-TKE) schemes. Validation of the LES using the available in situ turbulence measurements demonstrated that the LES provides robust information on turbulence variables in hurricane conditions (Chen, Bryan, et al., 2021). The observational estimates of momentum flux and eddy viscosity (French et al., 2007; Zhang & Drennan, 2012; Zhang, Marks, et al., 2011) are used in this study too. For more details of this framework, the related model setup, and the observational data, we refer interested readers to Chen, Bryan, et al. (2021).

2.2. Two Types of PBL Schemes

Two types of PBL schemes available in the CM1 model are tested in the SCM simulations in this study. The first type is the KPP schemes, which are known as the first-order, nonlocal closures. To be specific, "nonlocal" herein means parameterized turbulent fluxes are not necessarily related to local gradients in the mean fields and can include countergradient fluxes. The magnitude and vertical distribution of K_m in KPP schemes depend crucially

Table 1
Brief Description of Two Types of Planetary Boundary Layer (PBL) Schemes and the Effective Eddy Diffusivity K_m

Approximation	PBL scheme	$\overline{w'C'}$ and K_m ($z < h$)	Note
Nonlocal, first order	YSU	$\overline{w'C'} = -K_{\mathrm{YSU}}\frac{\partial \overline{C}}{\partial z} + K_{\mathrm{YSU}}\gamma_c + \overline{(w'C')}_h\left(\frac{z}{h}\right)^3$, $K_{\mathrm{YSU}} = kw_s z\left(1-\frac{z}{h}\right)^p, p = 2.$ $K_m = \frac{\sqrt{\overline{u'w'}^2+\overline{v'w'}^2}}{\sqrt{\left(\partial\overline{u}/\partial z\right)^2+\left(\partial\overline{v}/\partial z\right)^2}}$, w is vertical velocity, C is the prognostic variable, and w_s is the mixing-layer velocity scale.	Diagnosed h; p is shape parameter. Three terms on the right-hand side of the first equation denote downgradient, countergradient, and entrainment fluxes, respectively. Countergradient flux for u, v, and θ. Hong et al. (2006)
	GFS	Weakly unstable: $\overline{w'C'} = -K_m\left(\frac{\partial \overline{C}}{\partial z} - \gamma_c\right)$; strongly unstable: $\overline{w'C'} = -K_m\frac{\partial \overline{C}}{\partial z} + M_u\left(C_u - \overline{C}\right)\vert_{sfc}$. $K_m = kw_s z\alpha\left(1-\frac{z}{h}\right)^p, p = 2$, α is determined by capping K_m at 500-m height by $V_{500}/0.6$.	Diagnosed h; p is shape parameter. Countergradient flux γ_c for scalars only in weak unstable conditions. Han et al. (2016); Wang et al. (2018)
Nonlocal, 1.5 order	MYNN	$\overline{w'C'} = -K_m\frac{\partial C}{\partial z} + M_u\left(C_u - \overline{C}\right)\vert_{sfc}$. $K_m = LqS_m$, L denotes master mixing length, $q = \sqrt{2e}$, e denotes TKE, S_m is the similarity function.	$L^{-1} = L_s^{-1} + L_t^{-1} + L_b^{-1}$; L_s, L_t, L_b: surface-layer, turbulent, and buoyancy length scale; L is gradually replaced by the BouLac mixing length L_{BL} in the 300-m entrainment layer above the diagnosed boundary layer height (see details of *bl_mynn_mixlength* = 1). Nakanishi and Niino (2004, 2009); Olson et al. (2019)
	EDMF-TKE	$\overline{w'\phi'} = -K_\phi\left(\frac{\partial \overline{C}}{\partial z}\right) + M_u\left(C_u - \overline{C}\right)\vert_{sfc} + M_d\left(C_d - \overline{C}\right)\vert_{Sc}$, $K_m = L\sqrt{e}C_m$. The subscripts sfc and Sc denote surface driven and stratocumulus-top driven, respectively. C_m is prescribed within h.	$L^{-1} = L_s^{-1} + L_{\mathrm{BL}}^{-1}$; L_s, L_{BL}: surface-layer and BouLac length scales; L_{BL} is capped at 300 m above the surface layer. Han and Bretherton (2019)

Table 2
A Summary of Planetary Boundary Layer (PBL) Height Definitions in Different PBL Schemes

	PBL height definition	Additional information
YSU	Unstable conditions: Rib $= Ri_c = 0$	Rib $= \left[\frac{g}{\theta_{vs}}\left(\theta_{vh}-\theta_{v0}\right)h\right] / \left(u_h^2+v_h^2\right)$
GFS	Over ocean: Rib $= Ri_c = 0.25\left(10^{-7}R_0\right)^{-0.18}$, Rib $\in$ [0.15 0.35]	R_0: surface Rossby number
MYNN	A blending of z_i and z_{iTKE}	z_i: The height where θ_v exceeds the minimum θ_v in the bottom 200-m layer by 1 K (over water). z_{iTKE}: the height where TKE falls to 5% of the surface value.
EDMF-TKE	$h = \min\left(h_{w_u=0}, h_{Ri_c=0.25}\right)$	$h_{w_u=0}$ is the height where the surface-based updraft $w_u = 0$. $h_{Ri_c=0.25}$ is the height where the Rib $= Ri_c = 0.25$

on the diagnosed boundary layer height (e.g., Kepert, 2012). Two KPP schemes are selected in this study, that is, the YSU (Hong et al., 2006) and GFS schemes (Han et al., 2016; Wang et al., 2018). The YSU scheme is among the most popular PBL schemes in the Weather Research and Forecasting (WRF, Skamarock & Klemp, 2008) model for TC simulations (Kepert, 2012) and the GFS PBL scheme is used in the operational Hurricane WRF (HWRF, Gopalakrishnan et al., 2010) model.

As a first-order scheme, YSU does not involve any prognostic equations for the turbulence quantities. The subgrid-scale vertical turbulent fluxes below the diagnosed boundary layer height consist of downgradient, countergradient, and entrainment fluxes (see the three terms in Table 1). The diagnosed boundary layer height in YSU is defined by the level where the bulk Richardson number Rib equals a critical value Ri_c (see the definition in Table 2), and $Ri_c = 0$ wherever surface enthalpy fluxes are positive (i.e., unstable conditions).

The GFS scheme adopts a hybrid eddy-diffusivity mass-flux (EDMF) parameterization (Siebesma et al., 2007) that is specially designed for convective boundary layers, and a mass-flux parameterization for nonlocal turbulent fluxes is only used in "very unstable" boundary layer conditions. The stability is measured by a surface stability parameter $\zeta = z/L$, where z is the height of the lowest model level and L is Monin-Obukhov length, and ζ reflects the ratio of shear production of turbulence to buoyant production of turbulence. The boundary layer is "very unstable" when $\zeta < -0.5$, and "weakly unstable" for $-0.5 < \zeta < 0$. For the SCM simulations conducted in this study, the mass-flux function in GFS remains inactive, since the boundary layer in the model setup is "weakly unstable," and countergradient flux is used instead. In GFS, countergradient fluxes only apply to scalars. A closer examination of the LES and SCM simulations indicates that the near-surface layer in different high-wind conditions is nearly neutrally stratified, indicated by a small surface stability parameter $\zeta \approx -1 \times 10^{-3}$. Despite the presence of large enthalpy fluxes [O (1,000) W m^{-2}, not shown], high wind speeds and the associated strong vertical wind shear keep the hurricane boundary layer nearly neutrally stratified. Similar to YSU, the diagnosed boundary layer height in GFS is also defined by the critical bulk Richardson number Ri_c. The PBL code calculates the bulk Richardson number Rib between the surface and a specific model level starting from the bottom level and then gradually going upward until the Rib equals or is greater than Ri_c. The exact boundary layer height is then determined by performing a linear interpolation between the last two searching model levels. Over ocean $Ri_c = 0.25\left(10^{-7}R_0\right)^{-0.18}$ (see Table 2). The surface Rossby number $R_0 = \frac{U_{10}}{f_0 z_0}$, where U_{10} is the 10-m wind speed, f_0 is the Coriolis parameter, and z_0 is the surface roughness. The value of Ri_c is restricted within the range of 0.15–0.35 in the GFS scheme. A unique feature of GFS is that it incorporates a wind-dependent adjustment to the K_m profile based on aircraft observations at ~500 m height (Fovell & Bu, 2015; Wang et al., 2018; Zhang, Marks, et al., 2011). Specifically, the K_m value at 500-m height is capped by V_{500}/0.6, where V_{500} is the wind speed at $z =$ 500 m, and the K_m profile is adjusted accordingly to match the new K_m value at 500-m height.

The second type of PBL scheme is high-order closure schemes, that is, MYNN (Nakanishi & Niino, 2004, 2009) and EDMF-TKE (Han & Bretherton, 2019) schemes, which predict TKE and other turbulence quantities that are diagnosed from the TKE. Both MYNN and EDMF-KTE are used in NOAA's operational models: MYNN for High-Resolution Rapid Refresh model (Olson et al., 2019) and EDMF-TKE for FV3-based Hurricane Analysis and Forecast System (HAFS) and GFS models. The EDMF is available as an option in the MYNN scheme. In the recently released WRF model, version 4.2, the mass-flux component of the vertical turbulent flux in MYNN is gradually tapered off at high wind conditions when the EDMF option is turned on. As a consequence,

differences between the simulations with the mass flux component turning on and off are found to be negligible in hurricane conditions. For brevity, only the results without the activation of the mass-flux component are shown in the following section. Additionally, the level-3 closure of MYNN, that is, MYNN3.0, is evaluated in this study. Preliminary results show that results from MYNN3.0 and MYNN2.5 are very similar, although MYNN2.5 only predicts one second-order turbulent quantity (i.e., TKE) and thus excludes countergradient flux parameterizations. MYNN adopts a hybrid diagnostic boundary layer height that blends the potential temperature-based boundary layer height (z_i), which works well for convective boundary layers, and TKE-based boundary layer height ($z_{i\mathrm{TKE}}$), which is suitable for stable boundary layers (see a brief discussion in Table 2). Details for the hybrid diagnostic boundary layer height in MYNN were discussed in Olson et al. (2019).

In EDMF-TKE, the surface-driven mass flux is activated when $\zeta < -0.02$. While this triggering criterion is much more relaxed than that in GFS-EDMF, the small surface stability parameter $\zeta \approx -1 \times 10^{-3}$ in high-wind conditions as discussed above suggests the surface-driven mass flux remains inactive in the SCM simulations. EDMF-TKE only predicts one two-moment turbulent quantity (i.e., TKE) and thereby is analogous to the level-2.5 closure of MYNN. The PBL height definition in EDMF-TKE is different, however, which is taken as the lesser value of the height where the surface-based updraft velocity equals zero and a diagnosed PBL height based on critical Richardson number ($Ri_c = 0.25$ wherever positive surface enthalpy flux exists).

To reduce the sensitivity of the results to surface layer parameterizations, the GFDL surface layer scheme (Kurihara & Tuleya, 1974) from HWRF is used for all of the LESs and SCM simulations. The YSU, GFS-EDMF, and MYNN PBL codes and GFDL surface-layer code for this study are from version 4.2 of WRF. The EDMF-TKE code is taken from the NCAR Common Community Physics Package repository (https://github.com/NCAR/ccpp-physics). Of note, the settings for GFS-EDMF are identical to those in HWRF 4.0a. There is no coupling to an ocean or surface wave model.

3. Evaluation Results

A crucial diagnostic variable that is useful to compare different PBL schemes is the effective eddy viscosity K_m. This section evaluates the K_m profiles from different PBL schemes against LES results and examines the impact of K_m on the boundary layer wind profiles. The K_m from the LES is calculated as:

$$K_m = \frac{\sqrt{\overline{w'u'}^2 + \overline{w'v'}^2}}{\sqrt{\left(\partial\overline{u}/\partial z\right)^2 + \left(\partial\overline{v}/\partial z\right)^2}} + K_{\mathrm{mv}} + K_w \tag{1}$$

in which $\overline{w'u'}$ and $\overline{w'v'}$ are the domain-averaged resolved vertical turbulent fluxes related to radial and tangential winds, respectively; the $\partial\overline{u}/\partial z$ and $\partial\overline{v}/\partial z$ are vertical shear of the domain-averaged radial and tangential wind, respectively; K_{mv} denotes the standard subgrid-scale eddy viscosity, which plays a role mainly near the surface in the LES framework; and K_w denotes the near-wall eddy viscosity from the "two-part" subgrid turbulence model (Bryan et al., 2017). We found that the subgrid momentum fluxes related to K_{mv} and K_w are negligible except near the wall and in the entrainment layer in LES. Analogous formulations of effective K_m in the PBL schemes are listed in Table 1. Note in YSU K_m is different from its parameterized K_{YSU} since the vertical turbulent momentum flux includes the countergradient and entrainment fluxes. The effective K_m in YSU is calculated similarly as in the first term on the right-hand-side of Equation 1 except that $K_{\mathrm{mv}} = K_w = 0$.

Both the LESs and SCM simulations reach a quasi-steady state after $t = 2.5$ hr, and this study analyzes the steady-state solutions, which are averaged over the last 2 hours of the simulations (i.e., $t = 4$–6 hr). Figure 1a compares the K_m from the LES (black line) in V25 and the observed K_m from Zhang and Drennan (2012) (black dots) with relatively weak surface winds (18–30 m s^{-1}). The K_m profile of the LES is well within the range of observational values overall above 200 m, indicating an encouraging consistency between the LES and observations. Nevertheless, the scatter of observations is quite large, and LES values are consistently larger than the available observational estimates below 100 m. This comparison provides some confidence for the K_m evaluation in the higher-wind conditions (i.e., V35 and V45) using LESs (Figures 1b and 1c), although clearly more observations are needed in those conditions. Figures 1a–1c indicate that MYNN produces a K_m profile closest to the LES in all experiments below 1 km, despite a noticeable oscillation. The jagged K_m profile is attributed to the sharp profile of the stability function S_m in MYNN (not shown), and a fix to this issue is underway (Joseph Olson,

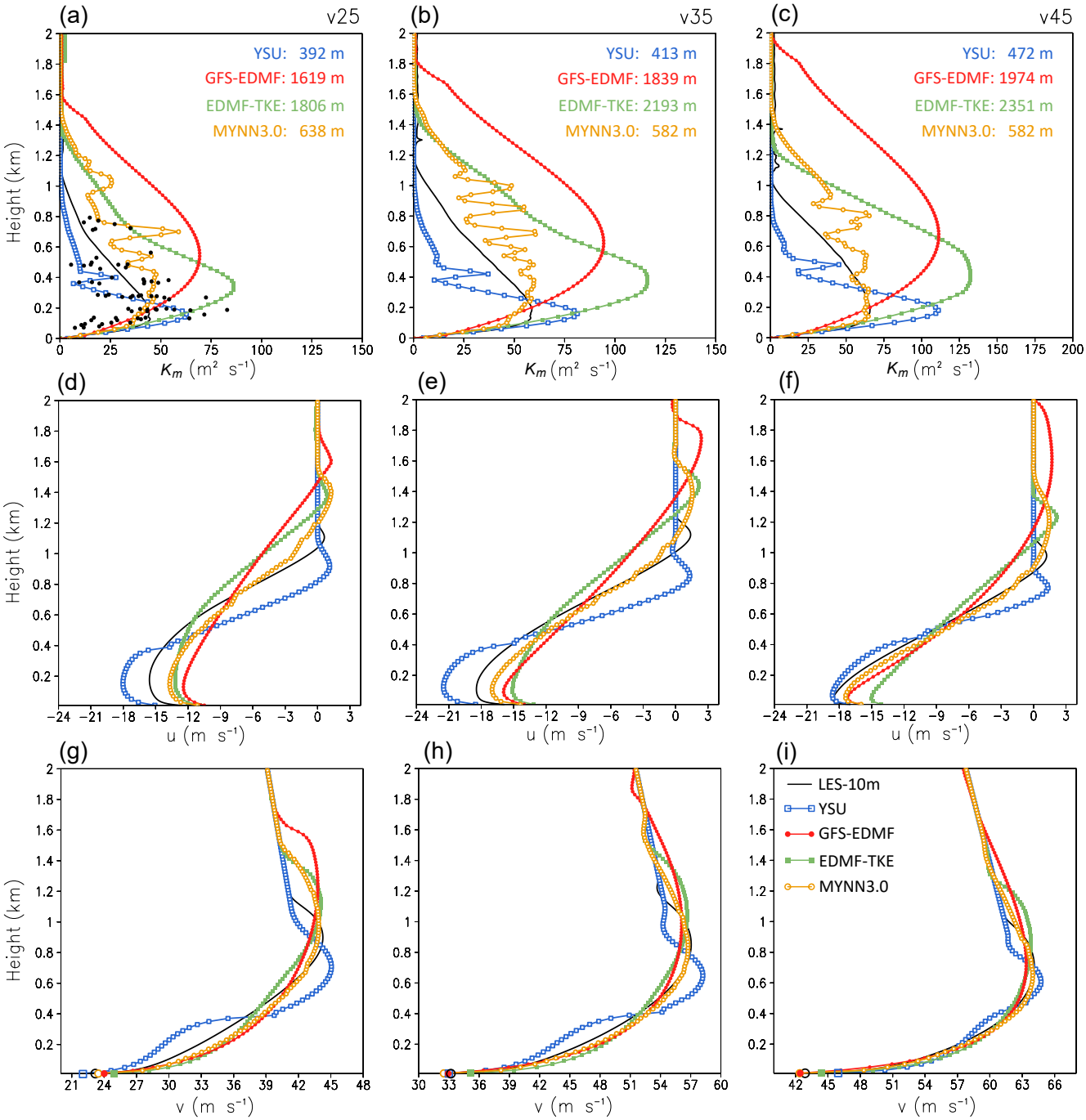

Figure 1. Vertical profiles of (a–c) effective K_m, (d–f) radial wind, and (g–i) tangential wind (m s^{-1}) from the large-eddy simulations (LES) and various planetary boundary layer (PBL) schemes [as indicated by the legend in panel (i)] for V25 (left), V35 (middle), and V45 (right). Black dots in (a) represent observations from Zhang and Drennan (2012). Markers at the *x* axis in (g–i) denote the 10-m tangential wind from LES and various PBL schemes. Diagnosed boundary layer height *h* from different schemes are shown in (a–c) and colored following the legend.

personal communication). EDMF-TKE produces larger K_m than LES in all experiments, with the maximum K_m a factor of 2 larger and the level of the maximum K_m ~200-m higher than the LES results. The maximum K_m in YSU appears at a similar height as in LES; however, compared to LES results, the K_m in YSU is larger below 300-m height and smaller above. In contrast, the GFS scheme produces an excessive vertical mixing scenario over a much deeper layer than the LES results, with the level of maximum K_m in GFS a factor of 3 higher in all

Table 3
Root Mean Square Error of Radial (u) and Tangential (v) Winds for Single-Column Model (SCM) Tests Using Different Planetary Boundary Layer Schemes (unit: m s^{-1})

	V25		V35		V45	
	u	*v*	*u*	*v*	*u*	*v*
YSU	3.4	2.5	3.7	2.2	1.9	1.2
GFS-EDMF	2.8	1.5	2.5	1.0	1.8	0.7
EDMF-TKE	2.3	1.5	2.7	1.4	2.5	0.9
MYNN3.0	1.5	1.0	1.3	0.7	0.8	0.4

Note. Results are averaged on the SCM model levels below 1 km. The smallest value in each column is in boldface.

experiments. These results suggest that the GFS scheme produces a much higher diagnostic boundary layer height h than YSU, since the level of the maximum K_m scales with h in KPP schemes (Kepert, 2012).

Figures 1a–1c show the h from different PBL schemes in V25, V35, and V45 experiments. Different PBL schemes clearly yield quite different h, with GFS and EDMF-TKE producing a much higher h than the other two schemes. Specifically, the h from YSU is more than a factor of 4 smaller than that from GFS. Compared to KPP schemes, the K_m in the high-order schemes is less dependent on h, as the vertical mixing from EDMF-TKE and MYNN extends in a similar depth despite the large differences in h between the two schemes. Of note, GFS produces weaker vertical mixing below the level of the maximum K_m (<600 m) than EDMF-TKE, which is attributable to the imposed wind-dependent adjustment to the K_m profile within the GFS code. Further discussions on this will be presented in Section 4.1.

Comparison of radial winds from PBL schemes and LES (Figures 1d–1f) shows that MYNN generally reproduces the LES inflow layer depth (height where inflow first vanishes) and matches the minimum value of u near the surface within 1–2 m s^{-1}, consistent with its best-matched K_m profile against the LES results in Figures 1a–1c. In comparison, the excessive vertical turbulent mixing in EDMF-TKE and GFS results in a too deep inflow layer, with the inflow strength in the V25 and V35 experiments much weaker than the LES results. In contrast, the less diffusive vertical turbulent mixing in YSU accounts for a shallower inflow layer with enhanced inflow strength near the surface than the LES results.

The tangential wind profile from the SCM tests exhibits less sensitivity to the K_m profile compared to the radial wind profile (Figures 1g–1i). The PBL schemes excluding YSU generally reproduce the LES tangential wind profile below 1 km. Not surprisingly, the tangential wind profile in MYNN is the best match to the LES counterpart in terms of reproducing the level of maximum tangential wind and the near-surface tangential wind. The non-representative structure of the tangential wind profile in YSU is most likely attributed to the significant underestimation of K_m above 300 m. A high bias of 2–3 m s^{-1} in the 10-m tangential wind is noted in YSU for V45 and also in EDMF-TKE for V35 and V45.

To quantitatively measure the performance of different PBL schemes, we calculate the root mean square error (RMSE) of radial and tangential winds for SCM tests, with LES treated as the benchmark. Table 3 shows the RMSE averaged on the SCM model levels below 1 km. In the three experiments, MYNN consistently produces the smallest RMSE ($\leq$1.5 m s^{-1}) for both radial and tangential winds compared to the other PBL schemes, which demonstrates its superior performance in simulating hurricane boundary layers.

4. Improvement to KPP PBL Schemes

4.1. K-Profile Adjustment

As discussed earlier, the K_m profile in the YSU and GFS schemes depends crucially on the diagnosed boundary layer height h, which is determined by the critical bulk Richardson number (Ri_c, see Table 2). As surface enthalpy fluxes remain positive in these experiments, $Ri_c = 0$ for YSU, and Ri_c is between 0.15 and 0.18 for GFS. Recall that in GFS Ri_c is a function of the surface Rossby number. As discussed in Section 3, the h from GFS is nearly a factor of 4 larger than that from YSU in all three experiments, which accounts for the large discrepancy in the K_m profile between these two schemes. In the original KPP form of K_m (O'Brien, 1970), h is the level at which K_m decreases to a local minimum and $\partial K_m/\partial z = 0$. Figures 1a–1c consistently demonstrate that the h is too low for YSU and too high for GFS compared to the LES results (i.e., $h \approx 1$ km). The following analysis will propose methods to improve these two KPP schemes in hurricane conditions.

Given that h is overestimated in GFS, we perform additional SCM tests with reduced Ri_c of 0.1, 0.05, and 0.025 for V45. Figure 2 shows that decreasing the Ri_c significantly reduces the h and meanwhile lowers the level of maximum K_m. The diagnosed h with $Ri_c = 0.025$ (the orange line in Figure 2) best matches the boundary layer height indicated by the LES. However, $Ri_c = 0.025$ is well beyond the capped range of Ri_c (0.15–0.35) in GFS, suggesting the definition of h in GFS does not work properly in hurricane conditions. A closer examination

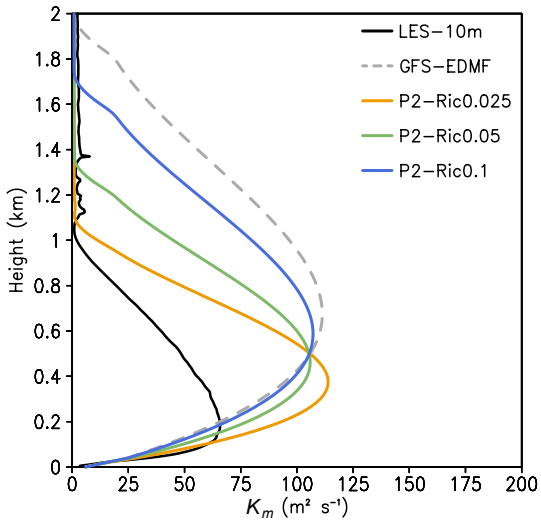

Figure 2. Vertical profiles of K_m ($m^2 s^{-1}$) from the large-eddy simulations (LES) (black), the original global forecast System (GFS) (dashed gray), and tuned GFS schemes with varied diagnosed boundary layer height for V45. Colored lines denote different Ri_c used in the tuned GFS as indicated by the legend.

indicates this issue is attributable to the excessive wind shear below the bottom model level, which significantly overwhelms the stratification effect and leads to a very small bulk Richardson number Rib (see the equation of Rib in Table 2). Thus, we adopt a different method of h that works well in all stability conditions, including high-wind conditions (Vogelezang & Holtslag, 1996). Instead of calculating the Rib from the surface to h, the "new" method calculates the $\mathrm{Rib}_{\mathrm{new}}$ from the bottom model layer to h:

$$\mathrm{Rib}_{\mathrm{new}} = \frac{\frac{g}{\theta_{vs}}(\theta_{vh} - \theta'_{vs})(h - z_s)}{(u_h - u_s)^2 + (v_h - v_s)^2 + 100u_*^2}, \quad (2)$$

where z_s is the height of the bottom model level, and u_s and v_s denote zonal and meridional winds at $z = z_s$, respectively. For stable and neutral boundary layers, $\theta'_{vs} = \theta_{vs}$, where θ_{vs} is the virtual potential temperature at $z = z_s$; for unstable conditions, $\theta'_{vs} = \theta_{vs} + \theta_T$ (Troen & Mahrt, 1986), where θ_T is virtual temperature excess near the surface. u_* denotes surface frictional velocity.

One important message taken from Figure 2 is that although with Ri_c = 0.025 GFS produces a similar h with LES, the maximum K_m in GFS remains much greater and further away from the surface than the LES results. The deviation of the structure of the adjusted K_m profile from the LES result (Figure 2b) indicates that the original "shape parameter" $p = 2$ (see definitions in Table 1) in YSU and GFS does not adequately describe the shape of the K_m profile in the hurricane boundary layer. For KPP PBL schemes, the maximum K_m appears at $z = h/(p + 1)$. Thus, p needs to be increased such that the level of maximum K_m decreases under a similar diagnosed h. Another benefit of increasing p is to reduce the maximum K_m (see Equation 14 of Kepert, 2012). After a series of tests, we find increasing p to 6 in both GFS and YSU better matches the K_m profile in LES.

It is worthwhile to note that when changing the diagnosed boundary layer height by adjusting Ri_c, the wind-capped K_m adjustment term in the GFS scheme (Fovell & Bu, 2015, see details in Section 2.2) can result in a discontinuous adjustment of the value of maximum K_m. Figure 2b shows that all K_m profiles from GFS converges at z = 500 m due to the wind-dependent adjustment term acting therein, while $Ri_c = 0.025$ corresponds to a larger maximum K_m than larger Ri_c values do. These results also demonstrate that the wind-dependent adjustment of K_m in GFS does not effectively fix the issue of boundary layer height and the shape of K_m profile in hurricane conditions. Given this, the wind-capped K_m adjustment is turned off in the experiments using the "new" definition of h in Equation 2 and $p = 6$.

Figure 3 shows an example of the tuned GFS with $p = 6$ and the new definition of h with different Ri_c (colored lines) against the original GFS (gray dashed line) for V45. Compared to the original GFS scheme, the tuned GFS scheme produces a shallower h (Figure 3a). Additionally, the diagnosed h with Ri_c = 0.15–0.35 from the tuned GFS shows a small spread, varying from 1.2 to 1.6 km in the steady state, which is in sharp contrast to the large sensitivity of the original GFS PBL height to the value of Ri_c as suggested by Figure 2b. These results prove that the new definition of h works well in the high-wind conditions. The diagnosed h with $Ri_c = 0.15$ (blue line in Figure 3a) is the closest match to the inflow layer depth from the LES (see Figure 3c), and the level of maximum K_m matches well with the LES as well (Figure 3b). Nevertheless, the K_m above the level of its maximum is considerably underestimated compared to the LES (cf. blue and black lines in Figure 3b), and the reduced vertical mixing leads to a shallower inflow layer depth and a lower level of the peak tangential wind (Figures 3c and 3d). The best tuned K_m profile with $p = 6$ occurs when $Ri_c = 0.35$ (orange line in Figure 3b), which is supported by the smallest RMSE averaged below 1 km (~11, not shown). Of note, the RMSE value for the best tuned K_m profile is more than a factor of 5 smaller than that from the original GFS (dashed gray line in Figure 3b), suggesting a substantial improvement to the K_m profile. With $p = 6$ and $Ri_c = 0.35$, the radial and tangential wind profiles from the tuned GFS scheme agree well with LES results, with a slight underestimation of the maximum inflow strength near the surface (Figures 3c and 3d). While the diagnosed h with the new definition is still greater than the LES result ($h \approx 1$ km), one implication of these findings is that in order to reproduce the LES results, the h

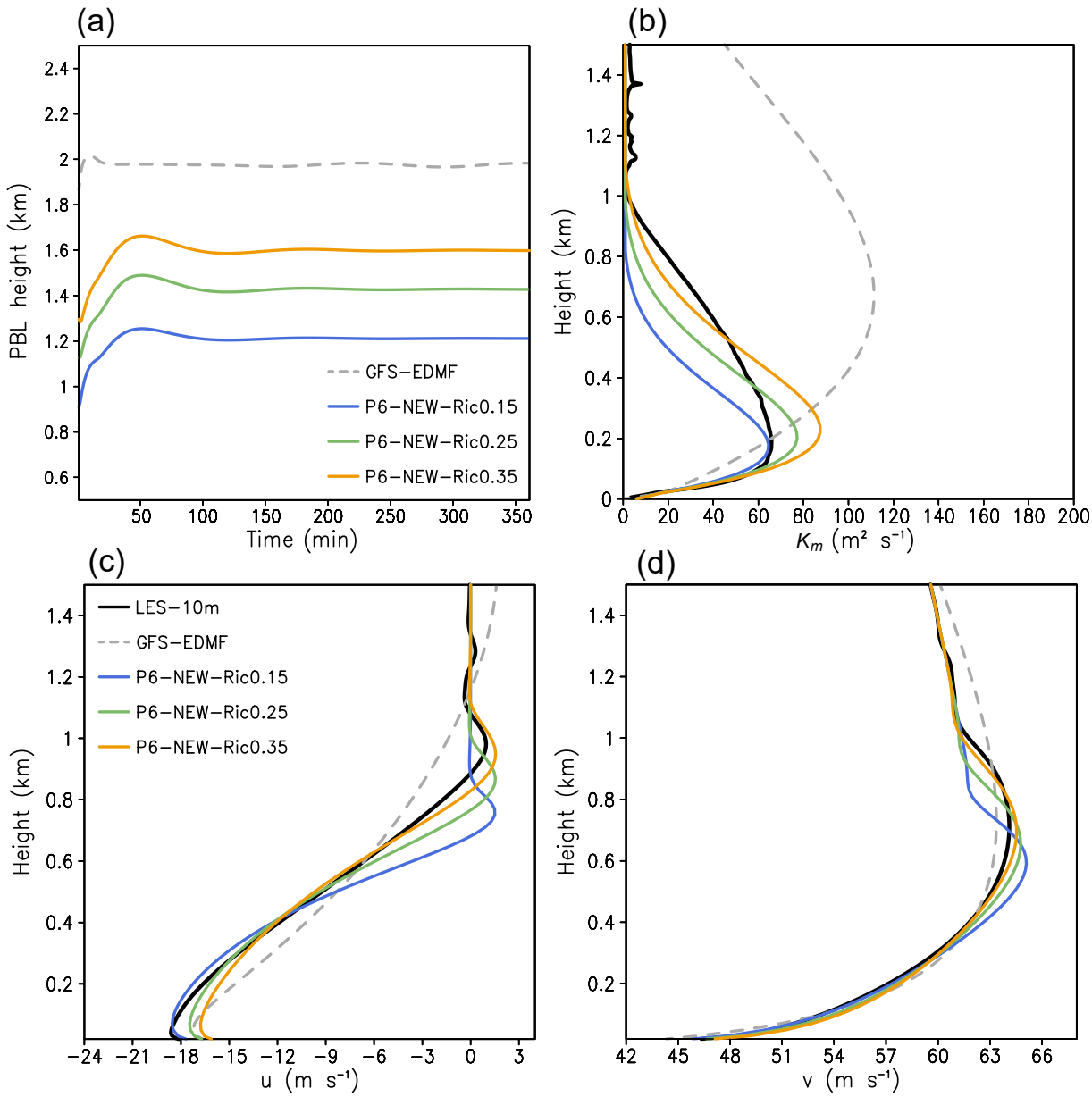

Figure 3. (a) Evolution of the diagnosed boundary layer height from the original global forecast System (GFS) with $p = 2$ (dashed gray), and tuned GFS schemes using $p = 6$ and the new planetary boundary layer (PBL) height definition for V45. Vertical profiles of (b) effective K_m ($m^2\ s^{-1}$), (c) radial wind ($m\ s^{-1}$), and (d) tangential wind ($m\ s^{-1}$) from the LES (black), original GFS with $p = 2$ (dashed gray), and tuned GFS schemes using $p = 6$ and new PBL height definition for V45. The legend for (b–d) is shown in panel (c). Colored lines in (a–d) denote different Ri_c used in the tuned GFS.

used in KPP schemes may not be equivalent to the physically meaningful boundary layer height (e.g., inflow layer depth) in hurricane conditions.

Similar adjustments to the profile in YSU are performed. One additional modification is turning off the countergradient fluxes of momentum in YSU such that the magnitude of the effective K_m is improved (or reduced; see the definition of effective K_m in Table 1). Recall that the GFS scheme does not include the countergradient fluxes of momentum while the YSU scheme does. Figure 4 evaluates the tuned GFS (red line) and YSU (blue line) using $p = 6$ and the new PBL height definition ($\mathrm{Rib}_{\mathrm{new}} = Ri_c = 0.35$) against LES (black line) in V25, V35, and V45 conditions. The tuned GFS and YSU schemes produce very similar results that match much better to the LES than the original schemes (cf. Figures 1 and 4). Although the maximum K_m in the tuned GFS and YSU differs from the LES, the shape of the K_m profile is much improved, especially in the surface layer and mid-upper boundary layer

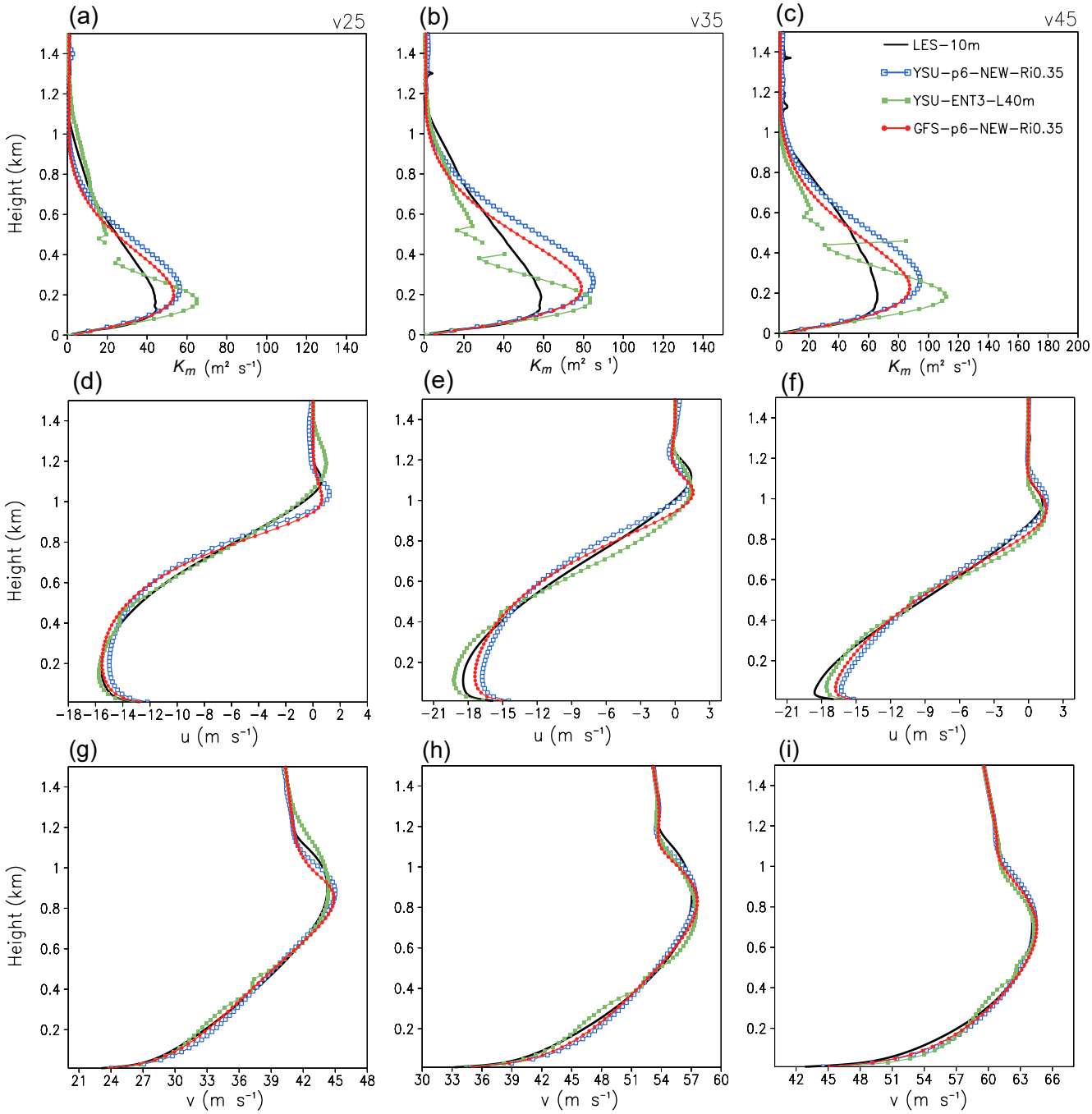

Figure 4. Vertical profiles of (a–c) K_m ($m^2\ s^{-1}$), and (d–f) radial wind ($m\ s^{-1}$), and (g–i) tangential wind ($m\ s^{-1}$) from the large-eddy simulations (LES) (black) and best-tuned Yonsei University (YSU) and global forecast System (GFS) schemes for V25 (left), V35 (middle), and V45 (right). The countergradient flux of momentum is turned off in the tuned YSU. Blue and red lines denote tuned YSU and GFS using $p = 6$ and the new PBL height definition ($Ri_c = 0.35$), respectively. The green line denotes the original YSU with modifications of tripled entrainment flux and l_∞ =40 m above the diagnosed boundary layer height (refer to the second approach in Section 4.2), and K_m above the boundary layer height is set to a missing value when its value is over 100 $m^{-2}\ s^{-1}$ in (a–c).

(cf. Figures 1a–1c and 4a–4c). The averaged RMSE of the K_m profile below 1 km from the tuned GFS and YSU schemes is reduced by 82% and 32%, respectively, compared to their original versions (not shown). Profiles of radial inflow and tangential wind in Figures 4d–4i further support the usage of $p = 6$ and $Ri_c = 0.35$ for YSU and GFS schemes, in terms of matching the inflow layer depth and the level of peak tangential wind, and in terms of reproducing the strongest inflow near the surface (cf. Figures 1d–1i and 4d–4i).

4.2. Another Approach to Improve the YSU Scheme

The original design of YSU adopts a shallow diagnosed boundary layer height h ($Ri_c = 0$ wherever positive surface enthalpy flux exists) and parameterizes the entrainment flux (see the equation with $\overline{(w'C')}_h$ in Table 1) separately, which are different from GFS. In YSU, K_m for $z > h$ is determined by a Louis-type scheme (Louis, 1979):

$$K_m = l^2 f_m(\mathrm{Rig}) \left(\sqrt{(\partial u/\partial z)^2 + (\partial v/\partial z)^2} \right), \tag{3}$$

in which f_m is the stability function in terms of the local gradient Richardson number Rig; for stably stratified free atmosphere (Rig > 0), $f_m(\mathrm{Rig}) = (1 + 2.1\mathrm{Rig})/(1 + 5\mathrm{Rig})^2$. $\sqrt{(\partial u/\partial z)^2 + (\partial v/\partial z)^2}$ is the vertical wind shear. l is the mixing length, and $l^{-1} = (kz)^{-1} + l_\infty^{-1}$, in which k is the von Kármán constant (= 0.4), and l_∞ is the asymptotic length scale, which represents the maximum allowable turbulence length scale above the surface layer. The different parameterizations in YSU compared to GFS suggest the possibility of another approach to improve the YSU scheme without the need to change the shape parameter p and PBL height definition. In the YSU scheme, $l_\infty = 30$ m. Recall that K_m (cf., Figures 1a–1c) in the original YSU is substantially underestimated above the diagnosed boundary layer height (≈400–500 m), and one can increase K_m therein by increasing l_∞. Figures 1a–1c also suggest that K_m from YSU is underestimated in the middle-to-upper part of the boundary layer, where the entrainment flux (see definition in Table 1) is a contributor to the total momentum flux. The entrainment flux relates to overshooting thermals in convective boundary layers and is characterized by a penetration depth (i.e., or the entrainment zone) that scales with the ratio of the convective velocity scale and the buoyancy frequency of the free troposphere. In YSU, the magnitude of entrainment flux is tuned empirically (Hong et al., 2006). Figures 5a–5c compare the vertical profiles of total momentum flux between LES (black) and YSU (blue), and also show the downgradient flux (green), countergradient flux (red), and entrainment flux (orange) in YSU. Clearly, the entrainment flux contributes a large portion of the total momentum flux in the middle-to-upper part of the boundary layer. Hereafter we perform additional SCM tests to assess whether modifications to the entrainment zone parameterization and to the asymptotic length scale l_∞ above h in YSU can better simulate the hurricane boundary layer.

Since entrainment flux parameterizations in YSU are developed and tuned empirically for convective boundary layers and the total momentum flux from YSU is underestimated compared to LES results in hurricane conditions, we conduct two experiments by doubling (green line in Figures 5d–5f) and tripling (red line in Figures 5d–5f) the entrainment flux in the original YSU with $p = 2$. Results indicate that the profile of the total momentum flux below the h is slightly improved compared to the original setting (blue line in Figures 5d–5f), most notably in the V25 and V35 experiments. However, momentum fluxes above the h ($z > 450$ m) remain underestimated, suggesting additional adjustments of the mixing length above the boundary layer height is necessary. The Louis-type mixing length derived from both LES experiments and observations (see Figure 11a in Chen, Bryan, et al., 2021) suggests a maximum value of ∼40 m above the h from YSU (i.e., $z > 500$ m). Given this, we adopt $l_\infty = 40$ m in the following analysis. Further tests indicate that by tripling the entrainment flux and setting $l_\infty = 40$ m simultaneously in the original YSU with $p = 2$ (referred to as YSU-EL, see orange line in Figures 5d–5f), YSU-EL reproduces the LES profiles of vertical momentum flux within 0.2 $m^2\ s^{-2}$ in all three experiments. In YSU-EL, K_m above the h of the original YSU increases with the larger l_∞, as seen from the differences between blue lines in Figures 1a–1c and green lines Figures 4a–4c, and matches better to the LES. Not surprisingly, the inflow depth and tangential wind profile in YSU-EL are much improved compared to the results of the original YSU (cf. Figures 4d–4i and Figures 1d–1i). Figures 4d–4f show that the maximum strength of boundary layer inflow in YSU-EL (green line) becomes even closer to the LES than the best tuned YSU with $p = 6$ (blue line). Of note, the vertical wind shear approaches zero near the diagnosed PBL height from YSU-EL, which accounts for the very large K_m value therein (see the missing portion of green lines in Figures 4a–4c).

5. Discussion

5.1. Why Does MYNN Perform Better in Hurricane Conditions?

The capability of MYNN to reproduce the wind and K_m profiles under different high-wind situations is in sharp contrast to the other PBL schemes (Figures 1a–1c and Table 3), especially the original KPP PBL schemes,

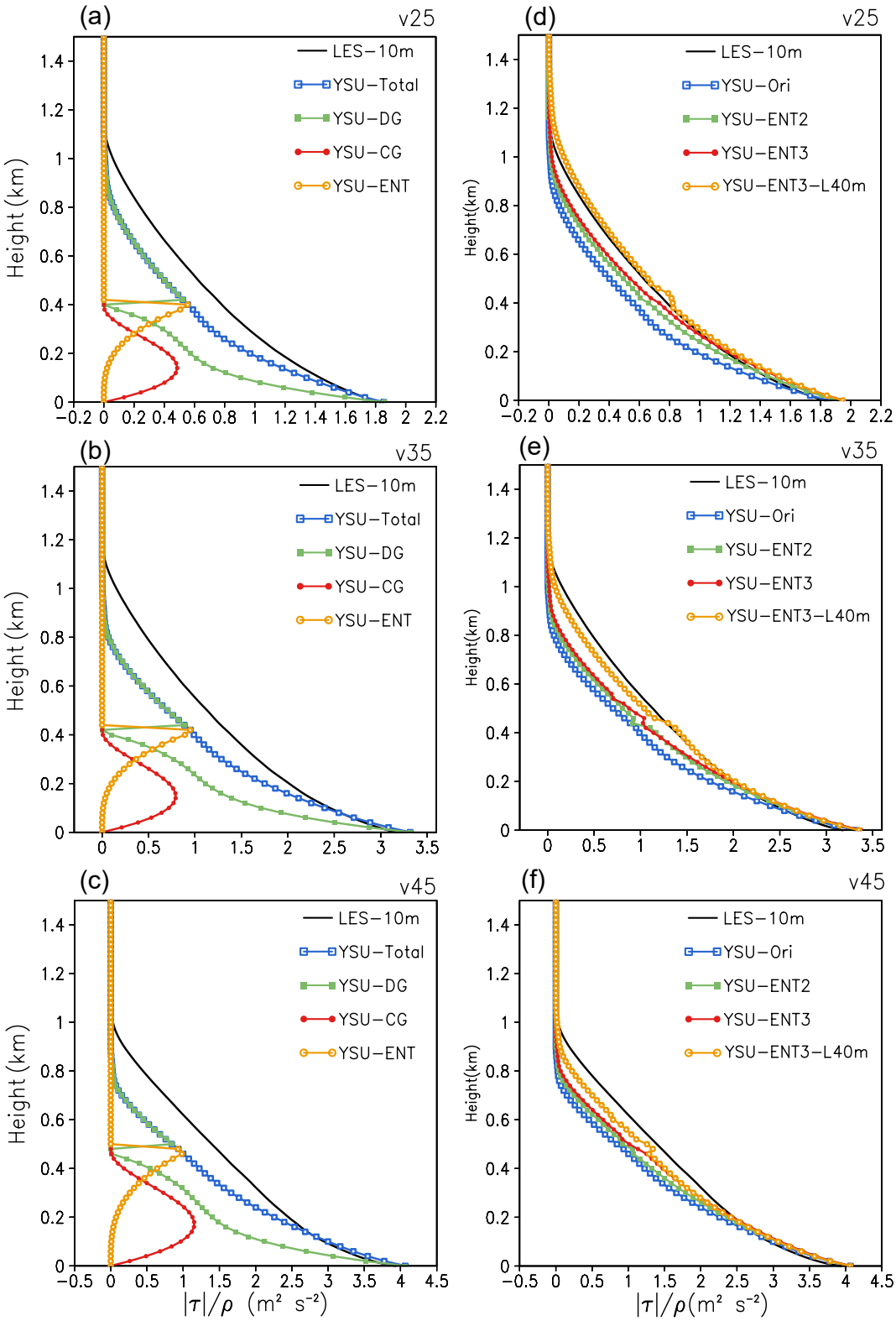

Figure 5. (a–c) Vertical profiles of momentum flux ($m^2\ s^{-2}$) from the original Yonsei University (YSU) averaged over $t = 4$–6 hr for V25, V35, and V45 experiments, respectively. The black and blue lines denote the large-eddy simulations (LES) and the original YSU, respectively. The green, red, and orange lines denote the downgradient flux, countergradient flux, and entrainment flux, respectively. (d–f) As in (a–c), but for the total vertical turbulent momentum flux from the LES (black), the original YSU (blue), the original YSU with the entrainment fluxes doubled (green) and tripled (red), and with entrainment fluxes tripled and $l_\infty = 40$ m (orange).

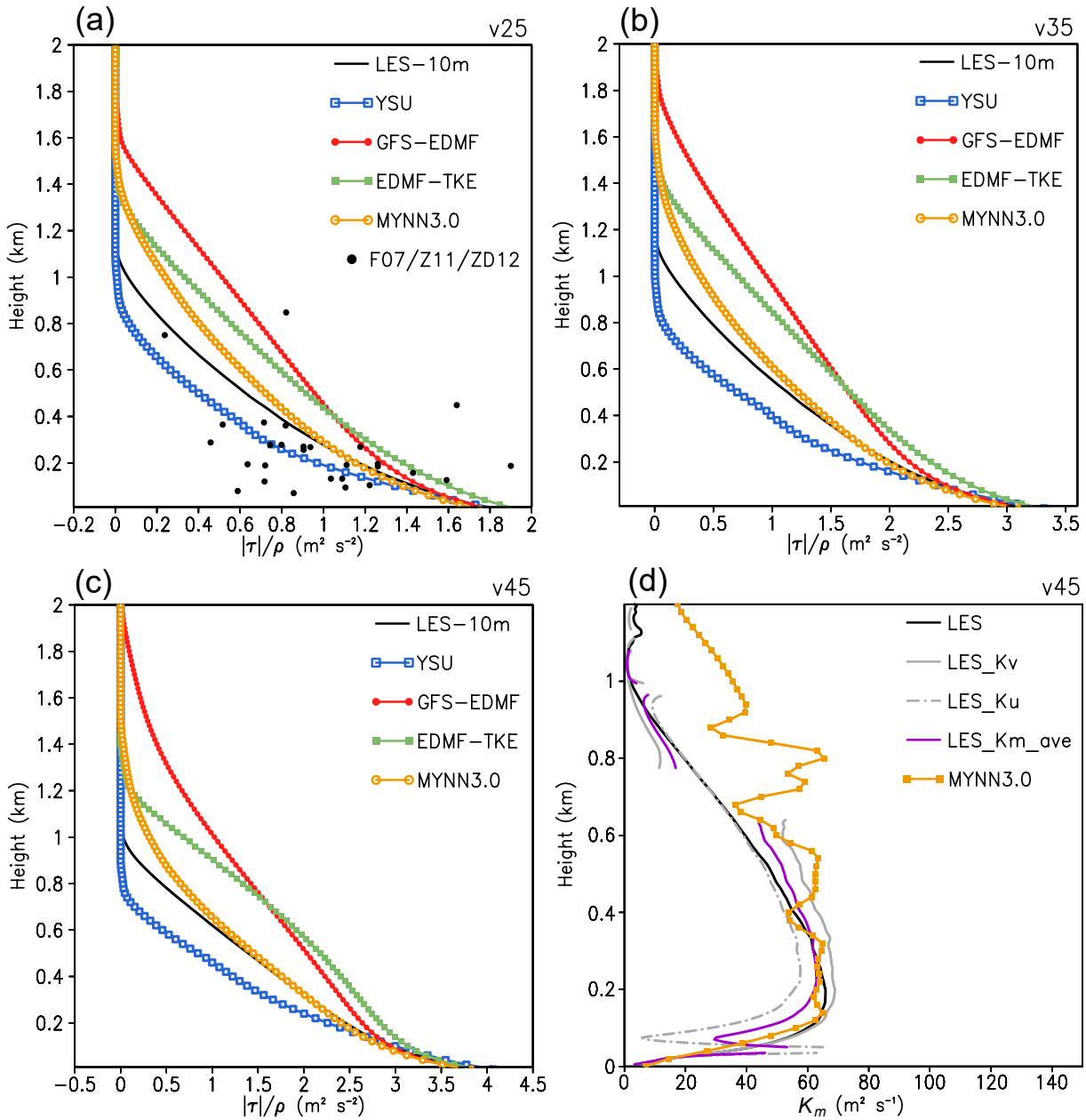

Figure 6. (a–c) The vertical profile of total vertical turbulent momentum flux ($m^2\ s^{-2}$) averaged over $t = 4$–$6\ hr$ for V25, V35, and V45 experiments, respectively. The dots in (a) denote in situ aircraft observations from (French et al., 2007; Zhang & Drennan, 2012; Zhang, Marks, et al., 2011). (d) Vertical profile of effective K_m ($m^2\ s^{-1}$, black), K_u (gray dash-dotted), K_v (gray dash), and the average of K_u and K_v (purple) from LES, as well as K_m from Mellor–Yamada–Nakanishi–Niino (MYNN) (orange) averaged over $t = 4$–$6\ hr$. K_u and K_v are set to a missing value when $|\partial\overline{u}/\partial z|$ and $|\partial\overline{v}/\partial z|$ are less than $3 \times 10^{-3}\ s^{-1}$.

suggesting the crudeness of the original KPP PBL schemes in representing turbulence characteristics within the hurricane boundary layer. This finding is consistent with the recommendation of high-order schemes for TC simulations by Kepert (2012), although Kepert's recommendation is based on the capability of the PBL schemes in producing the logarithmic wind profile in the surface layer. A closer examination of the K_m profile in MYNN indicates the K_m above 400-m height is larger than that in the LES (Figures 1a–1c). While the large K_m or vertical mixing can reduce the vertical gradient of the mean wind, the vertical turbulent momentum fluxes above 400-m height in MYNN remains slightly larger than the LES (Figures 6a–6c), suggesting the dominant role of K_m in determining the magnitude of vertical momentum fluxes. This result is also found for other PBL schemes (Figures 6a–6c). The magnitude of vertical turbulent momentum fluxes decreases with height more rapidly in

YSU than in other schemes, suggesting a stronger effect of frictional deceleration in YSU, which is consistent with the stronger inflow in YSU considering the subgradient nature of boundary layer inflow (Figures 1d–1f). The opposite phenomenon occurs in GFS and EDMF-TKE. As the inflow strength significantly impacts the relative importance between the radial advection of absolute angular momentum and frictional dissipation (Smith & Montgomery, 2015), these findings can help account for the frequently identified high bias of storm intensity in the model forecasts using the YSU scheme (Chunxi Zhang 2020; personal communication), and the low bias using the GFS scheme (Zhang et al., 2018).

Since the PBL tendency for momentum is determined by the vertical gradient of momentum flux, comparison of the profiles of momentum flux between LES and SCM tests provide additional insights into the performance of PBL schemes (Figure 6). The available observational estimates of the vertical turbulent momentum flux in hurricanes from the NOAA P3 aircraft (French et al., 2007; Zhang & Drennan, 2012; Zhang, Marks, et al., 2011) are also plotted as black dots in Figure 6a for a reference. These observational cases are selected when the observed total wind at the same vertical level was within 5 m s^{-1} of the domain-averaged mean wind from the LES, which is similar to the method used in Bryan et al. (2017). Additionally, observed momentum fluxes in the eyewall region are excluded since our evaluation framework is only applicable outside the eyewall. The selected cases only fit in the V25 condition.

Figure 6d further presents the effective vertical eddy viscosity determined only using the tangential (K_v) and radial winds (K_u) from the V45 LES. The definitions of K_v and K_u are:

$$K_v = \left| \frac{\overline{w'v'}}{\partial \overline{v}/\partial z} \right| + K_{\mathrm{mv}} \tag{4}$$

$$K_u = \left| \frac{\overline{w'u'}}{\partial \overline{u}/\partial z} \right| + K_{\mathrm{mv}} \tag{5}$$

respectively. The radial and tangential winds peak at approximately $z = 50$ m and $z = 700$ m heights (Figures 1f and 1i), respectively, where their vertical gradient approaches zero and vertical viscosity approaches infinity (see Equations 4 and 5). Considering this fact, K_v and K_u are set to a missing value when $|\partial \overline{v}/\partial z|$ and $|\partial \overline{u}/\partial z|$ are less than 3×10^{-3} s^{-1}. Interestingly, the K_v and K_u profiles derived from the LES are slightly different throughout the boundary layer (~1.0 km), with K_v typically larger than K_u. Therefore, the isotropy hypothesis in the parameterizations of these PBL schemes is invalid in the TC boundary layer, and it is technically inaccurate to use the same K_m in the governing equations for tendencies of tangential and radial wind (or meridional and zonal winds in the Cartesian coordinate) in TC simulations. This fact also suggests that tuning the K_m profile in the KPP schemes toward the effective K_m profile in the LES may not be an ultimate solution to improve these schemes.

Nevertheless, MYNN demonstrates its capability to reproduce the boundary layer wind profiles despite this non-isotropy issue. The K_m profile below 700 m from the MYNN is comparable to the average of K_v and K_u from the LES (see one example of V45 in Figure 6d). Aside from the advantage of high-order closures, the better performance of MYNN is in part attributed to its sophisticated mixing length parameterizations that can be adaptive to different environments (see the formulations of the master length scale in Table 1). In the boundary layer, the master length scale L or mixing length in MYNN is determined by a blending of three different length scales: surface-layer length scale L_s, turbulence length scale L_t, and buoyancy length scale L_b.

Figures 7a–7c show that in MYNN L (black line) is predominantly determined by L_s (green line) below 200 m in all experiments. The physical justification of L_s is that in the surface layer the size of turbulent eddies is proportional to the distance to the surface (e.g., Wyngaard, 2010, p. 215). In the 200–700 m layer, L_t (red line in Figures 7a–7c) is dominant. The definition of L_t is:

$$L_t = 0.23 \frac{\int_0^{h+\Delta z} qz\,\mathrm{d}z}{\int_0^{h+\Delta z} q\,\mathrm{d}z}, \tag{6}$$

where h is the diagnosed boundary layer height, Δz is the depth of entrainment layer (i.e., 300 m), and $q = (2 \cdot \mathrm{TKE})^{1/2}$. We find that the top of the entrainment level is very close to the diagnosed inflow layer depth from the LES. For example, $h = 582$ m for V35 (Figure 1b), and the top of the entrainment layer (i.e., 882 m) is

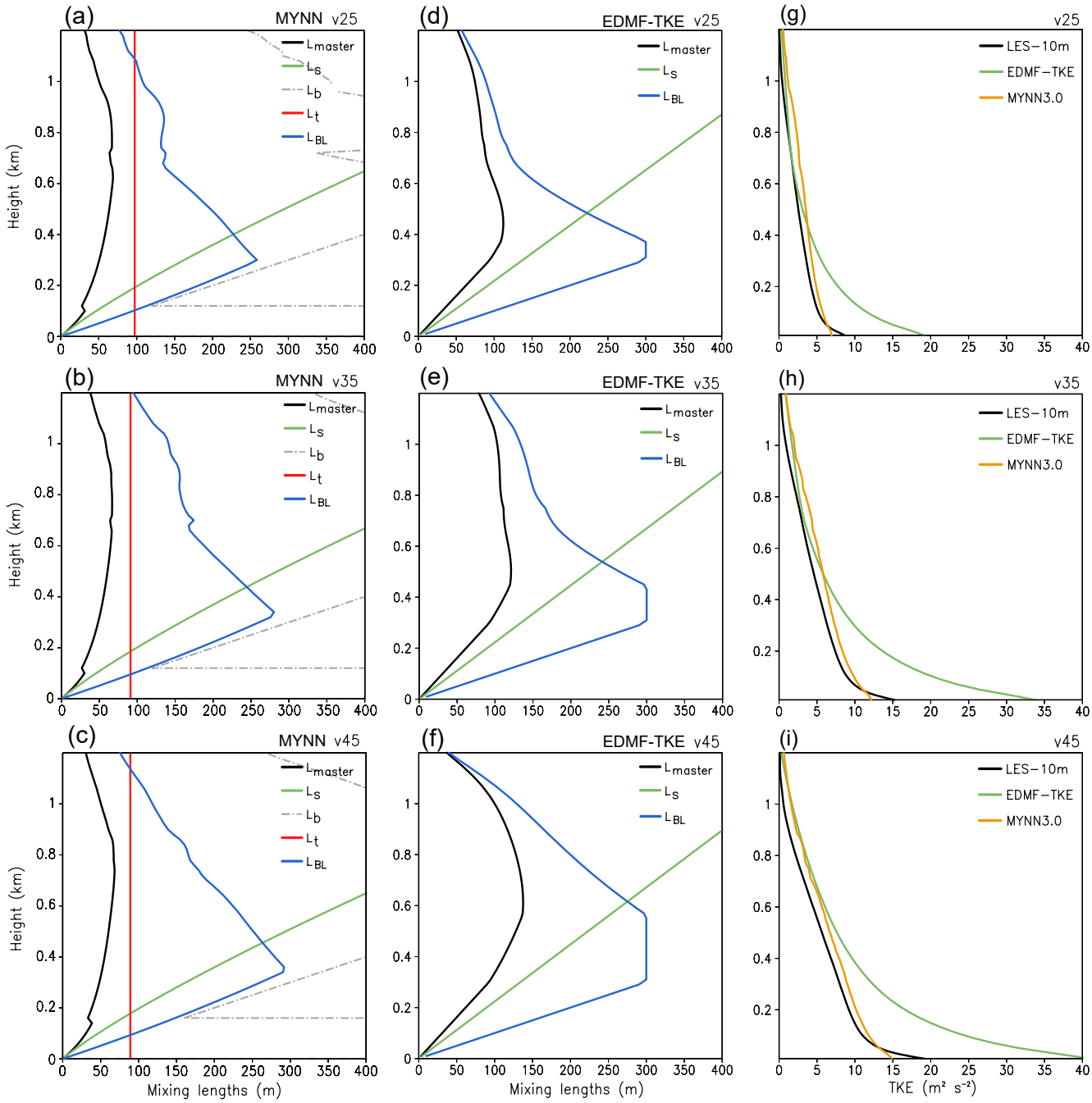

Figure 7. (a–c) Vertical profile of the master length scale (unit: m) of Mellor–Yamada–Nakanishi–Niino (MYNN) (black) that is a harmonic average of the surface-layer (green), buoyancy (gray), turbulence (red), and BouLac (blue) length scales in the V25, V35, and V45 experiments. (d–f) As in (a–c), but for master mixing length (black), surface-layer length scale (green), and BouLac length scale (blue) from eddy-diffusivity mass-flux-turbulence kinetic energy (EDMF-TKE). (g–i) Vertical profile of turbulence kinetic energy (unit: $m^2\ s^{-2}$) from LES (black), EDMF-TKE (green), and MYNN (red) for V25, V35, and V45, respectively.

close to the boundary layer height from the LES (~1 km, see the level of minimum value of K_m in Figure 1b). Thus, L_t can be considered as a measure of the mean size of turbulent eddies in the boundary layer. The magnitude of L_t varies with surface roughness and wind speeds, static stability, and boundary layer height. The L_b is found unimportant in the hurricane boundary layer (Figures 7a–7c), which is consistent with the notion that turbulence in the TC boundary layer is predominantly shear-driven (Bryan et al., 2017; Chen, Bryan, et al., 2021). The BouLac mixing length (i.e., $0.4 \times L_{BL}$) starts to play a role above 700 m (blue lines in Figures 7a–7c), as the BouLac mixing length and L consistently decrease with height therein. Above the boundary layer (>1 km), L is

mainly determined by the L_{BL} computed from two intermediate lengths, l_{up} and l_{down}, which represents the maximum possible distance traveled by an air parcel due to the loss of turbulent kinetic energy via buoyancy effects (i.e., to overcome the static stability) such that

$$\int_{z}^{z+l_{up}} \frac{g}{\theta(z)} \left[\theta\left(z'\right) - \theta(z)\right] dz' = e(z), \tag{7}$$

$$\int_{z-l_{down}}^{z} \frac{g}{\theta(z)} \left[\theta(z) - \theta\left(z'\right)\right] dz' = e(z),$$

where g and e denote the gravity parameter and TKE, respectively. $L_{BL} = \min\left(l_{up}, l_{down}\right)$. Results indicate that the sophisticated parameterization of mixing length in MYNN works well in different types of turbulent regimes in TC conditions, including the surface layer, lower-to-upper boundary layer, and above the boundary layer. Partly attributable to the sophisticated mixing length parameterizations, MYNN is capable of reproducing the LES TKE profiles within 2 m^2 s^{-2} above the near-surface layer in all experiments (see black and orange lines in Figures 7g–7i).

5.2. Issues With the EDMF-TKE PBL Scheme in Hurricane Conditions

In previous sections, we point out that the other TKE-based PBL scheme–i.e., EDMF-TKE–tends to produce excessive vertical mixing compared to the LES (e.g., Figures 6a–6c). EDMF-TKE adopts a different parametrization of mixing length compared to MYNN. In EDMF-TKE, the mixing length L is a blending of surface-layer length scale L_s and BouLac mixing length L_{BL}, and the maximum allowable value of L_{BL} is 300 m. EDMF-TKE also uses a different dissipation length scale l_d, that is, $l_d = \left(l_{up} l_{down}\right)^{1/2}$, while in MYNN $l_d = L$.

Results of SCM tests in Figures 7d–7f show that in all experiments the maximum L above the surface layer in EDMF-TKE is ∼100–150 m (black line), nearly a factor of 2 larger than the L in MYNN (i.e., ∼60 m) (black line in Figures 7a–7c). The different approach of mixing length and dissipation length scale in EDMF-TKE and MYNN affects shear production and dissipation of TKE and thereby affects the TKE profile in the boundary layer. Figures 7g–7i show that EDMF-TKE produces excessive TKE below $z = 500$ m (green line) compared to LES (black line); near the surface, the TKE in EDMF-TKE is a factor of 2 larger than the LES results, suggesting the shear production of TKE is overestimated and/or dissipation of TKE is underestimated. The notable inconsistency in the TKE profile between EDMF-TKE and LES was also reported for convective boundary layers (Han & Bretherton, 2019). The combined issues with the profiles of TKE and L account for the excessive eddy viscosity and momentum stress in EDMF-TKE (Figures 1a–1c and 6a–6c). We are investigating these issues in a forthcoming study.

6. Conclusions

PBL schemes in numerical models are mostly designed for non-hurricane conditions and their application to high-wind environments demands a closer examination. To this end, this study uses a recently developed modeling framework (Chen, Bryan, et al., 2021) that allows a small-domain LES and SCM tests using a PBL scheme under the same controlled thermodynamic conditions from actual category 4–5 hurricanes, and the LES output is used to evaluate the performance of two types of PBL schemes, that is, KPP and high-order PBL schemes.

Compared to the LES results, MYNN is capable of reproducing the vertical profiles of eddy viscosity K_m and boundary layer winds reasonably well under different high-wind situations, in part due to its high-order closure and sophisticated mixing length parameterizations. Further examination of MYNN recommends a "three-layer" strategy for the mixing length parameterization for the hurricane boundary layer: (a) the surface layer where the mixing length is proportional to the distance to the surface, (b) the lower-to-middle boundary layer where turbulence is primarily shear-driven and mixing length is parameterized as the mean turbulence size, and (c) the upper boundary layer and above where buoyancy effects on turbulence become more important. This three-layer strategy ideally characterizes three different turbulence regimes in the hurricane boundary layer and possibly frames how boundary layer turbulence structure should be analyzed in general.

In contrast, the high-order EDMF-TKE scheme adopts a different parameterization for mixing length such that the surface-layer length scale remains dominant below ~500 m. Thus, EDMF-TKE has a maximum mixing length in the boundary layer that nearly doubles that of MYNN. The differences in the mixing length contribute to a large TKE bias below 500 m in EDMF-TKE, with the near-surface TKE a factor of 2 larger than that in LES. The resulting excessive K_m causes a deeper inflow layer in EDMF-TKE than in MYNN and LES. A forthcoming study is underway to look into this issue and improve the EDMF-TKE scheme.

The KPP PBL schemes examined here (YSU and GFS) generally produce the least-accurate K_m and boundary layer wind profiles compared to the LES. The inaccurate boundary layer height and shape parameter p of the K_m profile are two factors driving this result. The inflow-layer structures in both YSU and GFS can be notably improved by increasing p from 2 to 6 and adopting a different definition of boundary layer height that works better in high-wind conditions. Turning off the countergradient fluxes in YSU further improves the structure of the radial and tangential wind profiles, suggesting that the parameterization of countergradient fluxes in YSU (originally designed to represent the overturning circulation spanning the full depth of convective boundary layers) should be revisited, at least for hurricane conditions. We also explore a second approach to improve YSU by using an asymptotic length scale of 40 m in the Louis-type parameterizations that operate above the diagnosed boundary layer, following the recommendation of the LES results and observations, and by tripling the entrainment flux within the diagnosed boundary layer height in YSU. The improved YSU scheme using the second approach can encouragingly reproduce LES wind profiles. One caveat of this study is that the modeling framework applies to the region outside the eyewall, and the proposed modifications to KPP PBL schemes are based on high-wind conditions outside the eyewall. We plan to further assess these modifications in the eyewall region by performing three-dimensional simulations, and examine the effects of these modifications on TC forecasts in the future. Assessing these modifications in various quadrants of sheared TC is also desirable in future work, which may invoke additional LES and SCM tests.

As a concluding note, the evaluation results in this study indicate that the high-order PBL schemes are physically more complete in terms of the generation and dissipation of turbulence and have a better chance to succeed in simulating TC boundary layers. Thus, we recommend high-order PBL schemes over KPP PBL schemes for TC simulations. We assessed the impact of TKE advection on TC simulations in an idealized study and highlighted that the TKE advection cannot be neglected in the TC simulations (Chen, Bryan, et al., 2021). With the ongoing efforts to improve the EDMF-TKE scheme, we plan to assess the effect of MYNN and improved EDMF-TKE schemes on TC intensity and structure forecasts in the framework of real-time operational models like NOAA's HAFS in the future.

Acknowledgments
The author would like to acknowledge high-performance computing support from Cheyenne (https://doi.org/10.5065/D6RX99HX) provided by NCAR's Computational and Information Systems Laboratory, sponsored by the National Science Foundation. The author is grateful to Dr. George Bryan for his constructive suggestions on the analysis and modeling setup, and to Drs. Robert Fovell and Scott Braun for the helpful communication on planetary boundary layer (PBL) schemes. The author appreciates the constructive comments and suggestions provided by Drs. Michael Fischer, Kyle Ahern, Frank Marks, and three anonymous reviewers that improve the clarity and quality of the analysis. This work was supported by award NA21OAR4320190 to the Northern Gulf Institute at Mississippi State University from NOAA's Office of Oceanic and Atmospheric Research, U.S. Department of Commerce. Xiaomin Chen was also supported by an NRC Research Associateship award.

Data Availability Statement

The CM1 model is available from https://www2.mmm.ucar.edu/people/bryan/cm1/getcode.html. The large-eddy simulations (LES) and single-column modeling experiments are available on NCAR's Cheyenne supercomputer, or by request.

References

Braun, S. A., & Tao, W.-K. (2000). Sensitivity of high-resolution simulations of Hurricane Bob (1991) to planetary boundary layer parameterizations. *Monthly Weather Review*, *128*(12), 3941–3961. https://doi.org/10.1175/1520-0493(2000)129<3941:SOHRSO>2.0.CO;2

Bryan, G. H., & Fritsch, J. M. (2002). A benchmark simulation for moist nonhydrostatic numerical models. *Monthly Weather Review*, *130*(12), 2917–2928. https://doi.org/10.1175/1520-0493(2002)130<2917:ABSFMN>2.0.CO;2

Bryan, G. H., Worsnop, R. P., Lundquist, J. K., & Zhang, J. A. (2017). A simple method for simulating wind profiles in the boundary layer of tropical cyclones. *Boundary-Layer Meteorology*, *162*(3), 475–502. https://doi.org/10.1007/s10546-016-0207-0

Chen, X., & Bryan, G. H. (2021). Role of advection of parameterized turbulence kinetic energy in idealized tropical cyclone simulations. *Journal of the Atmospheric Sciences*, *78*(11), 3559–3574. https://doi.org/10.1175/jas-d-21-0088.1

Chen, X., Bryan, G. H., Zhang, J. A., Cione, J. J., & Marks, F. D. (2021). A framework for simulating the tropical-cyclone boundary layer using large-eddy simulation and its use in evaluating PBL parameterizations. *Journal of the Atmospheric Sciences*, *78*(11), 3593–3611. https://doi.org/10.1175/jas-d-20-0227.1

Chen, X., Xue, M., Zhou, B., Fang, J., Zhang, J. A., & Marks, F. D. (2021). Effect of scale-aware planetary boundary layer schemes on tropical cyclone intensification and structural changes in the gray zone. *Monthly Weather Review*, *149*(7), 2079–2095. https://doi.org/10.1175/mwr-d-20-0297.1

Emanuel, K. (2017). Will global warming make hurricane forecasting more difficult? *Bulletin of the American Meteorological Society*, *98*(3), 495–501. https://doi.org/10.1175/BAMS-D-16-0134.1

Fovell, R. G., & Bu, Y. P. (2015). Improving HWRF track and intensity forecasts via model physics evaluation and tuning. In *DTC visitor program final report* (p. 28). Developmental Testbed Center. Retrieved from http://www.dtcenter.org/visitors/reports_2013/DTC_report_2013_Fovell.pdf

French, J. R., Drennan, W. M., Zhang, J. A., & Black, P. G. (2007). Turbulent fluxes in the hurricane boundary layer. Part I: Momentum flux. *Journal of the Atmospheric Sciences*, *64*(4), 1089–1102. https://doi.org/10.1175/JAS3887.1

Gopalakrishnan, S., Liu, Q., Marchok, T., Sheinin, D., Surgi, N., Tuleya, R., et al. (2010). In L. Bernardet (Ed.), *Hurricane weather and research and forecasting (HWRF) model scientific documentation* (p. 96). NOAA/ESRL Rep.

Gopalakrishnan, S. G., Marks, F., Zhang, J. A., Zhang, X., Bao, J.-W., & Tallapragada, V. (2013). A study of the impacts of vertical diffusion on the structure and intensity of the tropical cyclones using the high-resolution HWRF System. *Journal of the Atmospheric Sciences*, *70*(2), 524–541. https://doi.org/10.1175/JAS-D-11-0340.1

Han, J., & Bretherton, C. S. (2019). TKE-based moist eddy-diffusivity mass-flux (EDMF) parameterization for vertical turbulent mixing. *Weather and Forecasting*, *34*(4), 869–886. https://doi.org/10.1175/waf-d-18-0146.1

Han, J., Witek, M. L., Teixeira, J., Sun, R., Pan, H.-L., Fletcher, J. K., & Bretherton, C. S. (2016). Implementation in the NCEP GFS of a hybrid eddy-diffusivity mass-flux (EDMF) boundary layer parameterization with dissipative heating and modified stable boundary layer mixing. *Weather and Forecasting*, *31*(1), 341–352. https://doi.org/10.1175/WAF-D-15-0053.1

Hill, K. A., & Lackmann, G. M. (2009). Analysis of idealized tropical cyclone simulations using the weather research and forecasting model: Sensitivity to turbulence parameterization and grid spacing. *Monthly Weather Review*, *137*(2), 745–765. https://doi.org/10.1175/2008MWR2220.1

Hong, S.-Y., Noh, Y., & Dudhia, J. (2006). A new vertical diffusion package with an explicit treatment of entrainment processes. *Monthly Weather Review*, *134*(9), 2318–2341. https://doi.org/10.1175/MWR3199.1

Kepert, J. D. (2012). Choosing a boundary layer parameterization for tropical cyclone modeling. *Monthly Weather Review*, *140*(5), 1427–1445. https://doi.org/10.1175/MWR-D-11-00217.1

Kurihara, Y., & Tuleya, R. E. (1974). Structure of a tropical cyclone developed in a three-dimensional numerical simulation model. *Journal of the Atmospheric Sciences*,*31*(4))893–919. https://doi.org/10.1175/1520-0469(1974)031<0893:soatcd>2.0.co;2

Louis, J.-F. (1979). A parametric model of vertical eddy fluxes in the atmosphere. *Boundary-Layer Meteorology*, *17*(2), 187–202. https://doi.org/10.1007/BF00117978

Moeng, C.-H., & Sullivan, P. P. (1994). A comparison of shear- and buoyancy-driven planetary boundary layer flows. *Journal of the Atmospheric Sciences*, *51*(7), 999–1022. https://doi.org/10.1175/1520-0469(1994)051<0999:ACOSAB>2.0.CO;2

Nakanishi, M., & Niino, H. (2004). An improved mellor-yamada level-3 model with condensation physics: Its design and verification. *Boundary-Layer Meteorology*, *112*(1), 1–31. https://doi.org/10.1023/B:BOUN.0000020164.04146.98

Nakanishi, M., & Niino, H. (2009). Development of an improved turbulence closure model for the atmospheric boundary layer. *Journal of the Meteorological Society of Japan*, *87*(5), 895–912. https://doi.org/10.2151/jmsj.87.895

Noh, Y., Cheon, W. G., Hong, S. Y., & Raasch, S. (2003). Improvement of the K-profile model for the planetary boundary layer based on large eddy simulation data. *Boundary-Layer Meteorology*, *107*(2), 401–427. https://doi.org/10.1023/a:1022146015946

Nolan, D. S., Zhang, J. A., & Stern, D. P. (2009). Evaluation of planetary boundary layer parameterizations in tropical cyclones by comparison of in situ observations and high-resolution simulations of hurricane Isabel (2003). Part I: Initialization, maximum winds, and the outer-core boundary layer. *Monthly Weather Review*, *137*(11), 3651–3674. https://doi.org/10.1175/2009MWR2785.1

O'Brien, J. J. (1970). A note on the vertical structure of the eddy exchange coefficient in the planetary boundary layer. *Journal of the Atmospheric Sciences*, *27*(8), 1213–1215. https://doi.org/10.1175/1520-0469(1970)027<1213:ANOTVS>2.0.CO;2

Olson, J. B., Kenyon, J. S., Angevine, W. A., Brown, J. M., Pagowski, M., & Sušelj, K. (2019). A description of the MYNN-EDMF scheme and the coupling to other components in WRF-ARW. Technical Memorandum. Retrieved from https://repository.library.noaa.gov/view/noaa/19837

Siebesma, A. P., Soares, P. M. M., & Teixeira, J. (2007). A combined eddy-diffusivity mass-flux approach for the convective boundary layer. *Journal of the Atmospheric Sciences*, *64*(4), 1230–1248. https://doi.org/10.1175/JAS3888.1

Skamarock, W. C., & Klemp, J. B. (2008). A time-split nonhydrostatic atmospheric model for weather research and forecasting applications. *Journal of Computational Physics*, *227*(7), 3465–3485. https://doi.org/10.1016/j.jcp.2007.01.037

Smith, R. K., & Montgomery, M. T. (2015). Toward clarity on understanding tropical cyclone intensification. *Journal of the Atmospheric Sciences*, *72*(8), 3020–3031. https://doi.org/10.1175/JAS-D-15-0017.1

Smith, R. K., & Thomsen, G. L. (2010). Dependence of tropical-cyclone intensification on the boundary-layer representation in a numerical model. *Quarterly Journal of the Royal Meteorological Society*, *136*(652), 1671–1685. https://doi.org/10.1002/qj.687

Troen, I. B., & Mahrt, L. (1986). A simple model of the atmospheric boundary layer; sensitivity to surface evaporation. *Boundary-Layer Meteorology*, *37*(1), 129–148. https://doi.org/10.1007/BF00122760

Vogelezang, D. H. P., & Holtslag, A. A. M. (1996). Evaluation and model impacts of alternative boundary-layer height formulations. *Boundary-Layer Meteorology*, *81*(3), 245–269. https://doi.org/10.1007/BF02430331

Wang, W., Sippel, J. A., Abarca, S., Zhu, L., Liu, B., Zhang, Z., et al. (2018). Improving NCEP HWRF simulations of surface wind and inflow angle in the eyewall area. *Weather and Forecasting*, *33*(3), 887–898. https://doi.org/10.1175/WAF-D-17-0115.1

Wyngaard, J. (2010). *Turbulence in the atmosphere*. Cambridge University Press.

Zhang, J. A., & Drennan, W. M. (2012). An observational study of vertical eddy diffusivity in the hurricane boundary layer. *Journal of the Atmospheric Sciences*, *69*(11), 3223–3236. https://doi.org/10.1175/JAS-D-11-0348.1

Zhang, J. A., Marks, F. D., Montgomery, M. T., & Lorsolo, S. (2011). An estimation of turbulent characteristics in the low-level region of intense Hurricanes Allen (1980) and Hugo (1989). *Monthly Weather Review*, *139*(5), 1447–1462. https://doi.org/10.1175/2010MWR3435.1

Zhang, J. A., Marks, F. D., Sippel, J. A., Rogers, R. F., Zhang, X., Gopalakrishnan, S. G., et al. (2018). Evaluating the impact of improvement in the horizontal diffusion parameterization on hurricane prediction in the operational hurricane weather research and forecast (HWRF) model. *Weather and Forecasting*, *33*(1), 317–329. https://doi.org/10.1175/WAF-D-17-0097.1

Zhang, J. A., Nolan, D. S., Rogers, R. F., & Tallapragada, V. (2015). Evaluating the impact of improvements in the boundary layer parameterization on hurricane intensity and structure forecasts in HWRF. *Monthly Weather Review*, *143*(8), 3136–3155. https://doi.org/10.1175/MWR-D-14-00339.1

Zhang, J. A., Rogers, R. F., Nolan, D. S., & Marks, F. D. (2011). On the characteristic height scales of the hurricane boundary layer. *Monthly Weather Review*, *139*(8), 2523–2535. https://doi.org/10.1175/MWR-D-10-05017.1